NANO LETTERS

Letter

pubs.acs.org/NanoLett

Babinet-Inverted Optical Yagi–Uda Antenna for Unidirectional Radiation to Free Space

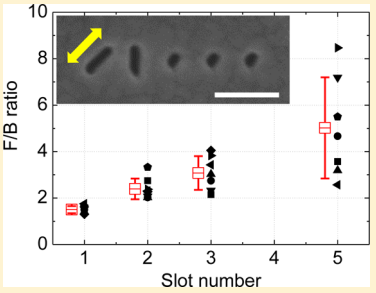
Jineun Kim,[†,§] Young-Geun Roh,[†,§] Sangmo Cheon,[†,§] Jong-Ho Choe,[‡] Jongcheon Lee,[†] Jaesoong Lee,[†] Heejeong Jeong,[†] Un Jeong Kim,[†] Yeonsang Park,*[,†] In Yong Song,[†] Q-Han Park,[‡] Sung Woo Hwang,[†] Kinam Kim,[†] and Chang-Won Lee*[,†]

[†]Samsung Advanced Institute of Technology, Yongin-si, Gyeonggi-do 446-712, Republic of Korea

[‡]Department of Physics, Korea University, Seoul 136-701, Republic of Korea

Supporting Information

ABSTRACT: Nanophotonics capable of directing radiation or enhancing quantum-emitter transition rates rely on plasmonic nanoantennas. We present here a novel Babinet-inverted magnetic-dipole-fed multislot optical Yagi–Uda antenna that exhibits highly unidirectional radiation to free space, achieved by engineering the relative phase of the interacting surface plasmon polaritons between the slot elements. The unique features of this nanoantenna can be harnessed for realizing energy transfer from one waveguide to another by working as a future "optical via".



KEYWORDS: *Plasmonic antenna, slot–slot interaction, Yagi–Uda, directional radiation, surface plasmon*

An optical antenna, a miniaturized analogy of a radio frequency (RF) antenna working in the optical regime, provides a new method of manipulating visible and infrared radiation at the nanoscale owing to strong light–matter interaction.[1−4] Various antenna functions across the optical spectrum have been realized, such as the transition rate enhancement of a quantum emitter,[5] enhanced photoresponse,[6] sensing of weak molecular signals,[7] nano-optical tweezers,[8] and beam forming.[9] In addition to the enhanced field effect, control of the radiation direction in the optical spectrum has also been successfully demonstrated by submicroscale Yagi–Uda antennas.[10,11] Optical Yagi–Uda antennas use a metal nanorod that acts as an electric dipole feed with additional nanorods for the reflector or directors.[12,13] An oscillating electric current of the feed element can be realized by the resonance-induced surface plasmon polariton (SPP) current along the length of the feed nanorod.

Aperture-type optical antennas, which can be considered as a Babinet-complementary counterpart of the rod-type optical antenna, have received little attention so far.[14,15] In the RF regime, a number of slot or leaky-wave antennas connected to waveguide structures have been studied for directional radiation control.[16] However, direct miniaturization of structures optimized for RF spectra is not possible for realizing efficient optical antenna operation because metals do not show perfect electrical conductor behavior over the optical spectrum.

A number of issues should be resolved to obtain efficient optical Yagi–Uda antennas based on aperture slots. Unlike rod-type antennas in which the oscillating electric dipole works as a feed, slot-type antennas require a resonance condition that can determine whether the feed is working as an electric dipole, magnetic dipole, or a mixed dipole.[4] Near-field interactions between rods are replaced by SPP exchange or quasi-cylindrical wave coupling between the slot elements in a slot-type antenna.[17] The geometry of an antenna based on multiple slots should be optimized by considering the intrinsic damping effect of SPPs, the substrate effect, and fabrication errors. In this Letter, we address all of these issues and demonstrate a novel aperture-type optical Yagi–Uda antenna that exhibits highly unidirectional radiation to free space.

Our work is different from previously studied structures for beam forming that were based on periodic nanoholes and slits to provide the interference effect.[20−22] Our antenna structure uses the resonance of the feed element, which allows incidence-angle-independent unidirectional radiation.[23] Furthermore, to discriminate pure antenna function from the radiation trapping effect due to the high refractive index substrate, we use our antenna as a free-space directional radiator. Our proposed structure represents the first optical antenna with a magnetic-dipole feed for free-space unidirectionality, which can potentially be embedded in an integrated plasmonic structure as a radiation router (optical via) or a chromatic discriminator.

The theoretical analysis of an aperture antenna operation is often based on Love's equivalence principle or the field equivalence principle (FEP) that enables a fast search of analytical solutions including the resonance conditions.[15] Application of the FEP to a narrow aperture slot made of a perfect electric conductor (PEC) on an infinite ground plane gives an analytical solution for the radiation due to the oscillating

Published: May 6, 2014

Downloaded via HANYANG UNIV on May 9, 2022 at 01:22:31 (UTC).
See https://pubs.acs.org/sharingguidelines for options on how to legitimately share published articles.

 © 2014 American Chemical Society dx.doi.org/10.1021/nl500062f | *Nano Lett.* 2014, 14, 3072−3078

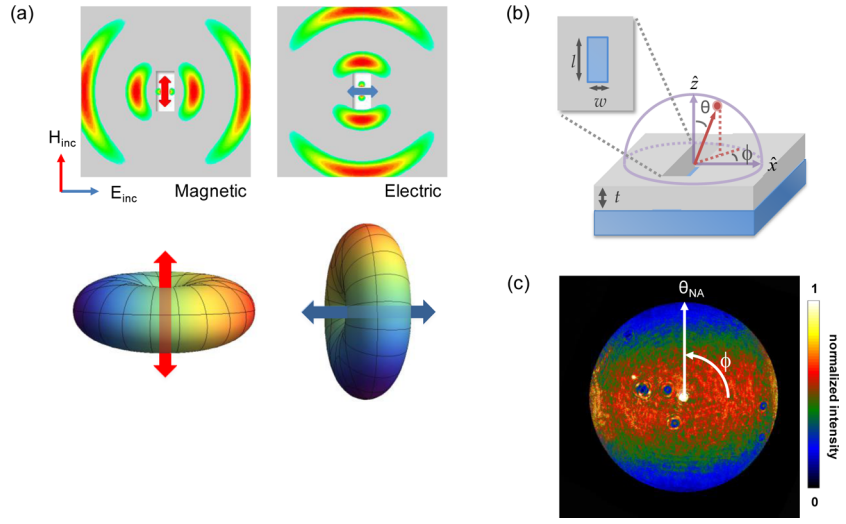


Figure 1. (a) Near-field radiation pattern in free space from a slot when a magnetic dipole is formed (top left) and when an electric dipole is formed (top right). The far-field radiation pattern of the corresponding field is shown underneath. (b) The coordinate system used to measure the radiation pattern from a single slot. The Fourier-plane image of the slot (or multislot antenna) is recorded as the intensity distribution projected onto a hemisphere with a sufficiently large radius surrounding the entire structure emitting the light. (c) A representative Fourier-plane image of the radiation measured from the single slot with l = 145 nm with 664 nm incident light. Two symmetric lobes are formed equally along the direction normal to the length of the slot similar to the simulation described in the Supporting Information, Figure S2.

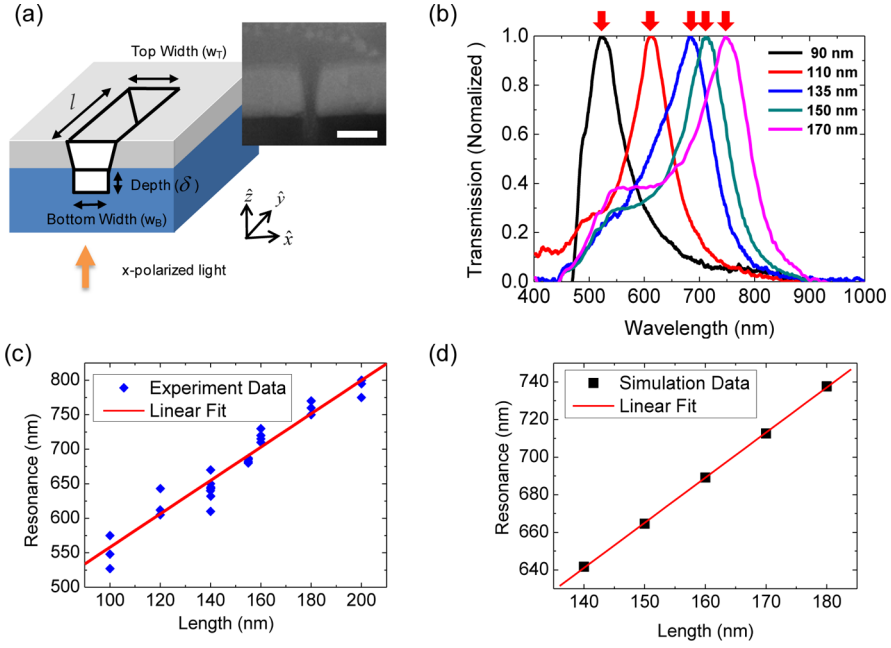


Figure 2. (a) Schematic of the simulated slot with the shape parameters. The slot has a trapezoidal-shaped cross section with shorter bottom width (w_B) and a longer top width (w_T). The depth of the trench into the substrate is δ. (Inset) Cross-sectional SEM image of the Ag single slot fabricated by focused ion beam (FIB) milling used in our experiment. The scale bar corresponds to 100 nm. The trapezoidal-shaped cross section and trench into the substrate can be observed. (b) Measured transmission spectra in the visible wavelength of single slots with lengths of 90−170 nm. The incident light is polarized normal to the length of the slot. The peak position, denoted by a red arrow, represents the resonance wavelength in each spectrum. (c) Resonance wavelength from the measured transmission spectra of a single slot on a glass substrate with various lengths (l). The linearity between the slot length and peak position is described by $\lambda = 2.4l + 315$ nm and shown in red line. This relation gives a design rule for single-slot resonance and a basic guideline for designing a multislot antenna with directionality. (d) Resonant wavelength from the simulated transmission spectra of the trapezoidal-shaped slot on the glass substrate with various lengths for t = 180 nm, w_T = 70 nm, w_B = 20 nm, and δ = 40 nm. A linear relation between the slot length and peak position can also be obtained: $\lambda_{FDTD} = 2.4l_{FDTD} + 305$ (nm).

magnetic current of the aperture. In practice, however, analytic solutions are elusive because of the strong dispersive and dissipative nature of metals with a finite conductivity. Therefore, it is important to know the leading order characteristics of the nature of the slot in terms of the radiation generator.[4]

Figure 1a shows the near- and far-field radiation patterns of a magnetic dipole and an electric dipole. If the slot induces a magnetic dipole at resonance, the near-field radiation should have an electric field component that is perpendicular to the length of the slot. If, instead, an electric dipole is induced across

dx.doi.org/10.1021/nl500062f | Nano Lett. 2014, 14, 3072−3078

the narrow slot width, then the electric field component of the near-field radiation is parallel to the length of the slot. As a result, the observed far-field patterns of the magnetic and electric dipoles are mutually orthogonal, which makes it easy to find the leading order of the induced dipole.

The coordinate system for a rectangular metal slot is sketched in Figure 1b with information about the θ and ϕ distributions of the radiation of a fabricated slot with a length of l = 145 nm and a width of w = 50 nm on a metal film with a thickness of t = 180 nm. The radiation pattern of a single slot is imaged at the back focal plane for a Fourier transformed image in transmission geometry after a proper apodization transformation and polarization filtering. Figure 1c shows the measured Fourier-plane image of a single slot as captured by an objective lens. The measured far-field electric field component is perpendicular to the length of the slot and has a near-uniform distribution along the x-axis. This confirms that the slot radiates as a magnetic dipole due to the resonantly excited magnetic current, regardless of the polarization and incidence angle of the irradiating laser (Supporting Information, Figure S2). Note that, when the polarization of the incident beam is not perfectly perpendicular to the output polarizer, a bright spot is formed at the center of the Fourier image due to the direct transmission.

Even though direct application of Babinet's principle to the optimized rod-type optical Yagi–Uda antenna does not provide an optimal design for slot-type antennas, several clues for obtaining an optimal design are provided. The operating principle of the Yagi–Uda antenna is based on the fact that each element behaves like a dipolar object and that the interactions between these elements determine the overall antenna performance. This means that the roles of the local feed and auxiliary elements in a Yagi–Uda antenna do not change as long as the slots behave as dipoles. However, a question arises as to what the operating principle is if the slots interact strongly. That is, is the operating principle of the Yagi–Uda antenna still valid with respect to the assumption that each slot represents a single elemental object? For extraordinary transmission, it has been known that the interactions between slots occur through SPP exchange or quasi-cylindrical waves. However, it is not clear if an optical antenna based on multiple slots can be built following the conventional antenna operation principle. We address this issue by analyzing the relative electromagnetic phases in the slots and show that a phase analysis can be applied to a wide range of geometrical variations of our multislot optical antennas. Practical limitations due to imperfect fabrication techniques can be compensated for during the simulation stage, and we show that systematic finite-difference time-domain (FDTD) simulations indeed compensate for the differences between the designed and the fabricated structures.

Our approach for determining the best performing optical multislot antenna is as follows. First, we start by searching for the resonance condition of a narrow slot aperture. Because fabricated slots less than 100 nm in width do not have a rectangular cross section, we design a more realistic modified slot structure, as shown in Figure 2a. Second, based on the resonance condition of the slot as a feed element, we add a reflector slot to induce unidirectional radiation. We rotate the reflector slot by 45° and illuminate the antenna with a laser beam that is linearly polarized in a direction parallel to the reflector slot so that only the feed slot is excited.[10] Due to the angular difference between the feed and the reflector, there are two possible configurations, which we discuss here, and we show that optimizing the feed radiation is more important than optimizing passive elements. Third, director slots are added to improve the unidirectional properties. For each process, we compare the performance of the fabricated and simulated structures.

A slot aperture made of a PEC has a dipolar resonance wavelength λ that is approximately two times the slot length l. However, a slot made of a real metal (such as Ag) illuminated by a visible wavelength shows the following modified linear relationship between the resonant wavelength and the slot length due to the finite skin depth:[24]

$$\lambda = al + b \tag{1}$$

Due to fabrication limitations, two additional effects need be considered: the effects of the substrate and the cross-sectional shape, which depend strongly on the fabrication method. The inset of Figure 2a shows a cross-sectional scanning electron microscope (SEM) image of a typical single slot used in our experiment. The SEM image shows that the fabricated slot has an isosceles trapezoid shape with an additional trench in the substrate. The width of the upper aperture at the air interface is 70 nm, while the width of the bottom aperture at the quartz substrate is 30 nm.

To determine an accurate relationship between the resonant wavelength and the slot length, we measured the transmission spectra of single slots with lengths of 90–170 nm (Figure 2b). In this experiment, the width in the middle of the slot and the thickness of the silver film were fixed at 50 and 180 nm, respectively. By plotting the resonance wavelength against the slot length (Figure 2c), we obtained the following linear relation between λ and l:

$$\lambda = 2.4l + 315\ (\text{nm}) \tag{2}$$

which has a similar form to the resonance condition of a rod-type antenna.[25]

In the three-dimensional (3D) FDTD calculations to simulate the actual slot shape, we used a simplified slot geometry with a trapezoidal-shaped cross section modeled using three additional parameters, the bottom side width (w_B), top width (w_T), and depth of the trench into the substrate (δ), as shown in Figure 2a. We first changed w_B while keeping δ at zero, so that the constraint $w_B = 100 - w_T$ holds. In this case, the resonance peaks of the spectra are red-shifted, and the slope of eq 2 increases as w_B decreases. This result arises from the plasmonic effect in a rectangular slot.[26,27] We then considered the effect of over-etching the substrate, i.e., a nonzero δ. The resonance of the slot with fixed w_B shows a blue shift, and the slope of eq 1 decreased as δ increased. This result arises from the effective dielectric constant of the trenched substrate decreasing as δ increases.[28]

By combining these two results, we found that the transmission spectra were best fitted when w_T = 70 nm, w_B = 20 nm, and δ = 40 nm:

$$\lambda_{FDTD} = 2.4l_{FDTD} + 305\ (\text{nm}) \tag{3}$$

as shown in Figure 2d. Note that the y-intercept of the slope in the FDTD simulation exceeds the experimental intercept by 10 nm. This arises from the round-edge effect of a real slot, which makes the effective length of the slot larger than the simulated one.

The design of an efficient multislot antenna is based on understanding the nature of the interaction between two slots when one slot acts as a feed slot to drive the other. We chose a 145 nm feed length to study the nanoantenna function at 664 nm (red) according to the linear relation in eq 3. There are two main factors to consider in the geometric configurations of two slots.

dx.doi.org/10.1021/nl500062f | Nano Lett. 2014, 14, 3072–3078

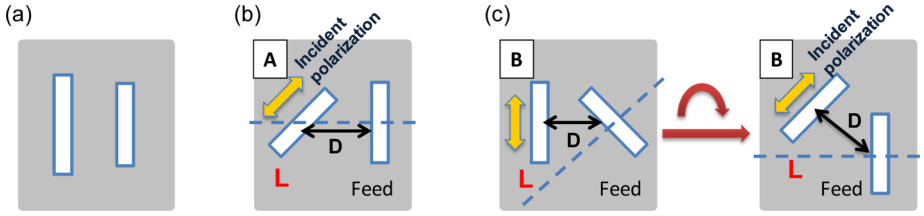


Figure 3. (a) Geometric configuration of two slots. Two parallel slots have the strongest interaction when they are located face-to-face. However, the linearly polarized incident laser can then excite both slots. Rotating one slot by 45° with respect to the other produces two possible configurations. (b,c) Two configurations for a two-slot antenna when one slot is tilted by 45° with respect to the length direction of the feed. Type A is shown in (b) and type B is shown in (c). The length of the second slot is denoted as L, and the distance between the two elements as D. The polarization of the incident and transmitted light are indicated by the blue arrow. Type A is a structure in which the center of the second tilted slot is aligned with the normal direction of the feed. Type B is a structure in which the center of the feed is aligned with the normal direction of the second tilted slot. A clockwise-rotated configuration of (c) is also shown for the convenience of the FDTD simulation. The dashed blue lines represent the radiation direction of the feed slot.

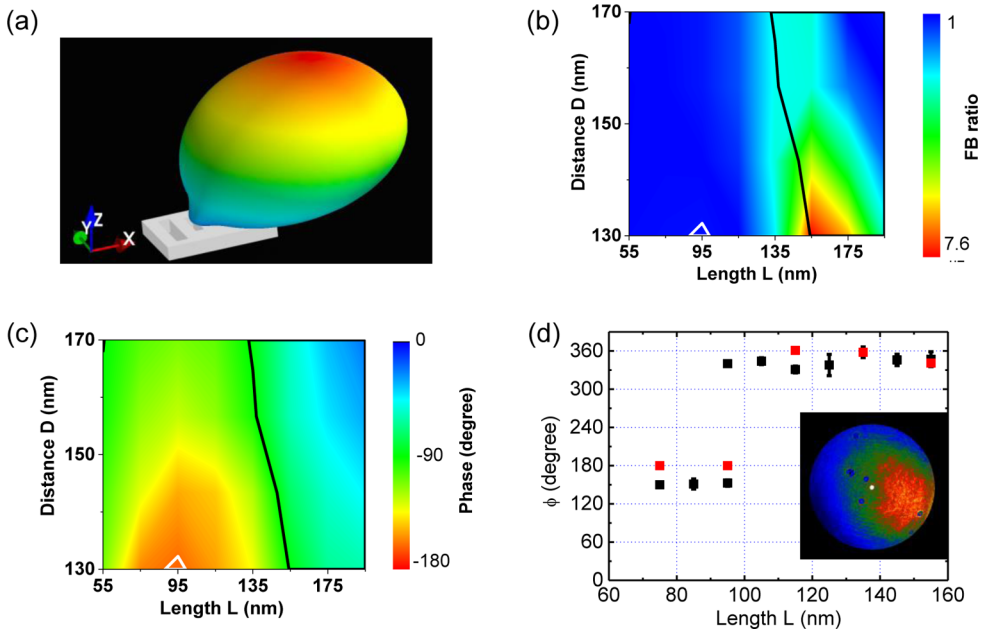


Figure 4. (a) Simulated far-field pattern from a two-slot antenna. (b) FB ratio contour plot as a function of L and D of the reflector for a given feed with a 145 nm length. The maximum FB ratio exists around the region of L = 155 nm and D = 130 nm. The black (white) line denotes a phase difference of −90° (−170°) between the feed and the additional slot obtained from the phase map in (c). (c) The phase difference between two slots. The phase difference of −90° is indicated by the black line, where the second slot acts as a reflector (backward light from the slots is out of phase). (d) The ϕ angles with maximum intensity (ϕ_{max}) as a function of L. For $75 \leq L \leq 95$ nm, ϕ_{max} changes from 150° to 330°. This plot shows that the tilted second slot works as a reflector when L > 100 nm and as a "weak" director when L < 100 nm. The black (red) rectangles indicate the ϕ_{max} obtained from the experiment (simulation). The inset in (d) shows a typical Fourier-plane image of the radiation of two-slot antenna for L = 155 nm and D = 130 nm. The antenna radiates light directed to $\phi_{max} \sim 330°$, i.e., forward, which shows clearly that the second slot acts as a good reflector.

First, the coupling between slots leads to energy exchange through SPPs or the evanescent coupling of electromagnetic energy.[12,17] Since both SPPs and diffracted electromagnetic energy through the slots mostly propagates perpendicular to the length of the slot,[29] it is readily expected that the coupling between the two slots is the strongest when they are facing each other, as shown in Figure 3a.[30]

In this configuration, however, both the feed and the auxiliary slots are excited by polarized illumination. Therefore, we use a polarization selection trick by rotating the feed element by 45° with respect to the other slot and the incident polarization.[10] Since a parallel polarized beam does not excite the slot structure, the polarization of the incident laser beam is always parallel to the auxiliary slot, leading to excitation of the feed slot only. This configuration is very effective for realizing local feeding of the Yagi−Uda structure without using a local quantum source.

Tilting the feed slot in the Yagi−Uda structure gives rise to another degree of freedom for designing an optimal antenna structure. For the two-slot case, there are two possible configurations. Let us assume a reflector slot is located to the left of the feed slot. When the reflector is tilted with respect to the feed slot as in Figure 3b, we refer to this structure as "type A". When the feed is tilted with respect to the reflector as shown in Figure 3c, we refer to this as "type B". Type A is the case in which the reflector (or director in other multislot cases) is located at the surface normal of the feed. Type B is the case in which the feed is located at the surface normal of the reflector (or director). Physically, type A is optimized for maximal transfer of the SPP energy *from the feed to the reflector/director*. In contrast, type B is optimized for *maximal reflection of the reflector* and *maximal directing power of the director*. We note that the incident laser polarization is always parallel to the reflector slot in both type A and B antennas. These two configurations lead to different

dx.doi.org/10.1021/nl500062f | *Nano Lett.* 2014, 14, 3072−3078

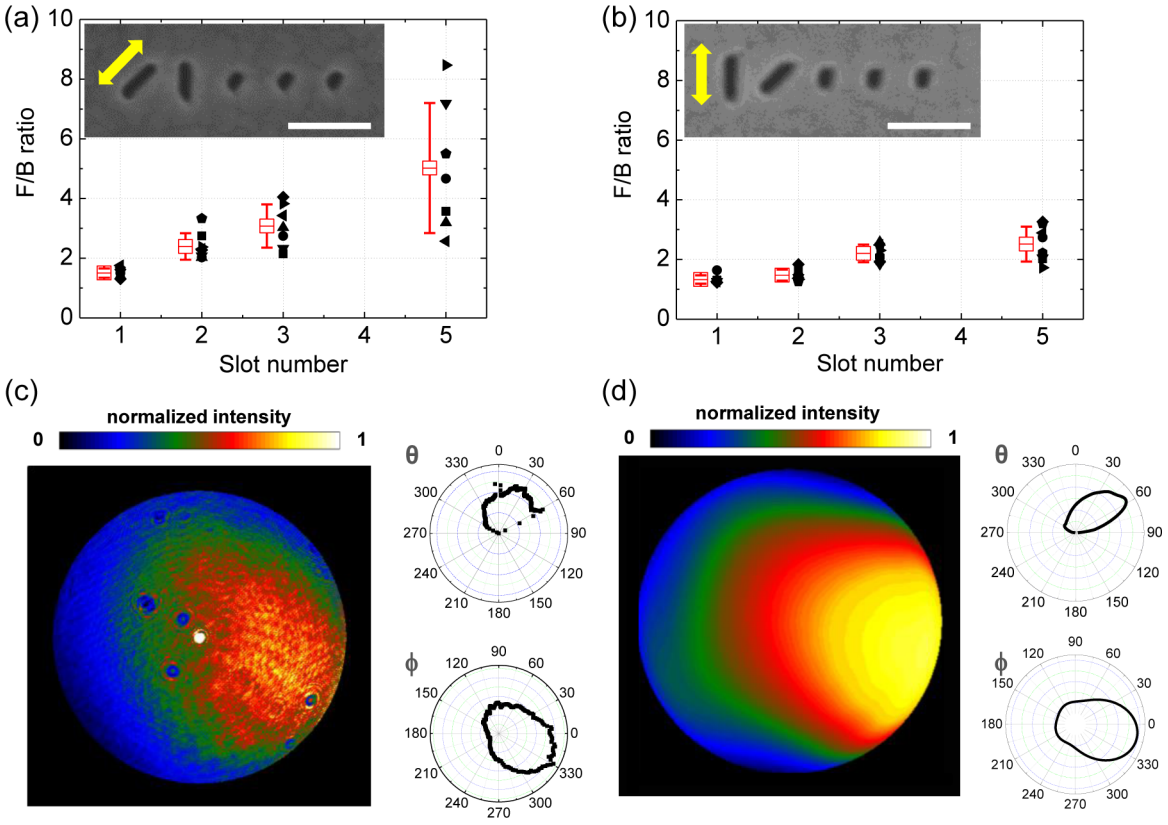


Figure 5. (a) Measured FB ratios of the type-A antennas as a function of the number of slots. (b) Measured FB ratios of the type-B antennas (complementary structure of the previously reported Yagi–Uda antenna). SEM images of each type of antenna are shown in the insets (scale bars: 200 nm). The black symbols denote the FB ratios measured from 28 devices (7 devices for each antenna configuration). The red rectangles denote the average FB ratio of each case. As the number of slots increases, the average FB ratios and the deviation increase. The maximum FB ratio obtained is 8.5 (9.2 dB) from a five-slot antenna. The average FB ratio of the type-B antenna is ~50% smaller than that of the type-A antenna. (c) The measured Fourier-plane image (color plot) and the radiation patterns in θ and ϕ. The image is taken from the best type-A antenna with five elements. (d) The simulated antenna radiation pattern of the antenna with the same five-slot geometry.

optimization conditions for reflector and directors and also affect optimal performance of each type.

In addition to the directions of the two elements, the length of the reflector element (L) and the distance between the two elements (D) need to be decided. We performed full 3D FDTD simulations[18] for a range of D and L values: we varied D from 130 to 180 nm and L from 55 to 195 nm (Supporting Information, Figure S4a). These values were determined from our fabrication ranges. Figure 4a shows a 3D view of the far-field radiation pattern obtained from a near-to-far-field transformation of the two-slot antenna radiation. By choosing an appropriate set of D and L, efficient unidirectional radiation to free space can be obtained. For a more comprehensive overview, we present a contour map of the front-to-back (FB) ratios as a function of D and L in Figure 4b. Large FB ratios are obtained when $L > 120$ nm, and the FB ratio increases with decreasing D in the same region. The maximum FB ratio for the type-A antenna, 7.6 (8.8 dB), is expected with L = 155 nm and D = 130 nm, which provides a condition for the best reflector operation of the second slot. We note that, unlike rod-type Yagi–Uda antennas, the optimal condition for D = 130 nm is smaller than one-quarter of the wavelength of the free-space electromagnetic wave (664/4 nm = 166 nm) or the wavelength of the SPP ($\lambda_{spp}/4 = [(\varepsilon_0 + \varepsilon_1)/(\varepsilon_0\varepsilon_1)]^{1/2}/4 = 0.97\lambda_0/4 = 161$ nm, where $\varepsilon_0 = 1.0$ for air and $\varepsilon_1 = -17.7 + i1.13$ for silver at $\lambda_0 = 664$ nm). The optimal distance between the feed and the reflector of a rod-type Yagi–Uda structure is given by the destructive interference condition via the free-space interaction of the rods, but slot-type antennas are strongly coupled by SPP waves propagating at the metal/dielectric interface and inside the finite-thickness slot aperture.

Similar FDTD simulations were performed for type-B antennas (Supporting Information, Figure S4b). The maximum FB ratio of 6.1 (7.8 dB) was obtained when L = 165 nm and D = 130 nm. Even though the optimal D and L values do not change much for both antenna types, the maximum FB ratio of the type-B antenna is slightly smaller than that of type-A antenna. As inferred from the geometrical analysis above, we find that the type-A configuration provides a better antenna performance owing to optimal SPP energy transfer from the feed to the auxiliary elements.

To gain a more comprehensive physical insight into the aperture-type antenna design, we investigated the phase relationship between the elements. Optimal conditions for rod-type RF and optical Yagi–Uda antenna designs have revealed that the spacing between the feed and the reflector should be one-quarter of the wavelength for destructive interference. The spacing between directors is a more complicated parameter and is known to depend on the number and lengths of the elements.[16] It is evident that direct conversion to a Babinet-complementary geometry does not necessarily provide an optimal design for an aperture antenna. However, we show that the physical principle of the Yagi–Uda antenna still holds. In a narrow rectangular slot, the y-component of the electric field (E_y) is weakly formed, and therefore the effective magnetic current density (M_{eff}) is

dx.doi.org/10.1021/nl500062f | Nano Lett. 2014, 14, 3072–3078

generated mostly from the x-component of the electric field (E_x) given by $\vec{M}_{\text{eff}} = -2\hat{n} \times \vec{E} = -2\hat{z} \times \vec{E} = -2(\hat{y}E_x - \hat{x}E_y) \approx -2\hat{y}E_x$.[15,31] FDTD simulations show that the y-component of the electric field can indeed be neglected because its magnitude is almost 10 times smaller than that of the x-component (see Section 2 in the Supporting Information). The phase of the field inside the slot is also uniform, and therefore, the phase of the x-component of the electric field is a leading order candidate for characterizing the magnetic currents corresponding to each slot.

We calculated the phase values at the center of the slots and plotted the difference as a function of D and L, as shown in Figure 4c. Here, the phase difference is defined as the phase of the second slot element minus that of the feed. When the phase difference approaches −90°, electromagnetic waves radiating from the feed destructively interfere with those reflected from the second slot to the left, resulting in unidirectional radiation toward the right-hand side of the feed. If we compare Figure 4b,c, the maximum FB ratio region coincides with the region of the −90° phase difference, which is denoted by the black lines. This results show that the phase analysis used in RF Yagi−Uda antenna theory still holds when the phase of the slot is properly defined as an object characterizing each individual slot.

We examined the two-slot devices more closely for L values of 55−195 nm while keeping D fixed at 130 nm. Figure 4d shows the azimuthal angle (ϕ_{max}) at the maximum intensity taken from the measured Fourier-plane images as a function of L. The black and red rectangles indicate the measured and simulated ϕ_{max} values, respectively. Both the measurement and the simulation show a jump from $\phi_{\text{max}} = 360°$ to $\phi_{\text{max}} = 180°$ near $L = 95$ nm, suggesting that the mode of the two-slot configuration changes from the reflector to the director; this in turn suggests that the two-slot combination can also be considered as a feed director. The inset of Figure 4d shows a representative Fourier-plane image measured from the device with $L = 155$ nm and $D = 130$ nm (reflector condition). These measured data experimentally demonstrate that the phase matching condition adapted from the RF antenna can also be applied to find the optimal reflector of the optical nanoantenna. The director condition corresponding to the phase difference of −270°, however, could not be found within the given ranges of D and L. The best director condition we found in Figure 4 was $D = 130$ nm and $L = 95$ nm, with the largest phase difference of −170° as denoted by the white lines in Figure 4b,c. Therefore, a single director is not sufficient for directional radiation, which in turn implies that multiple slots will show better antenna performance.

To show the enhancement in the directivity with more directors, three- and five-element slot antennas were designed and fabricated (Sections 4 and 5 in the Supporting Information). To examine the fundamental antenna behavior independent of the fabrication errors, more than 7 antenna structures with the same geometry were prepared and measured. For the three-slot antenna, we found that a structure with a reflector of $L_{\text{refl}} = 155$ nm and $D_{\text{refl}} = 130$ nm and a director of $L_{\text{dir}} = 95$ nm and $D_{\text{dir}} = 140$ nm provided the largest FB ratio for a feed of $L_{\text{feed}} = 145$ nm (Section 4 and Figure S11 in the Supporting Information). For the five-slot antenna, we further optimized the geometrical factors of an additional two director slots based on the three-slot antenna structure. We note that the five-slot antenna with a feed, reflector, and three directors becomes a complementary structure of the previously reported Yagi−Uda nanoantenna.[10,11] Similar to the two-slot case, multiple slots with reflector or director elements tilted by 45° with respect to the feed allow for two possible configurations. For type-A antennas, the reflector and director slots are tilted with respect to the feed maximizing the interaction of SPPs generated by the feed, as shown in the inset of Figure 5a. The measured FB ratios from individual type-A antenna structures are plotted in Figure 5a as a function of the number of slots. In general, multiple slots show better unidirectional performance on average, even though variations from individual structures become large. The best FB ratio from a type-A antenna was 8.5 (9.2 dB).

We also prepared and measured type-B structures, which are complementary structures of those previously reported.[10] Unlike type A, only the feed slot is tilted, while all of the other elements remain orthogonal to the entire antenna structure, as shown in the inset of Figure 5b. In this case, the direction of the radiation from the feed is not aligned in the direction of the auxiliary elements. However, the interaction between the feed and other elements is enough to generate unidirectional radiation. A similar optimization procedure was performed to find the D and L values for the maximum FB ratio (Section 5 and Figure S14 in the Supporting Information). The measured FB ratios obtained from the type-B slot antennas are plotted in Figure 5b as a function of the number of slots. The maximum FB ratio of 2.6 (4.1 dB) was obtained when $L_{\text{refl}} = 165$ nm and $D_{\text{refl}} = 130$ nm for the reflector and $L_{\text{dir}} = 95$ nm and $D_{\text{dir}} = 150$ nm for the director. The average FB ratios of the type-B antennas are, however, ∼50% smaller than those of the type-A antennas. Even though the FB ratios of the type-B antennas might increase slightly with different choices of D and L, we find that the type-A antennas generally produced relatively larger FB ratios (Sections 4 and 5 and Figures S15 and S16 in the Supporting Information).

We note that the feed of our aperture Yagi−Uda antenna radiates energy in the form of either SPPs or near-field radiation. Since the feed slot acts as a magnetic dipole moment, the direction of the generated energy is mostly normal to the feed length. This leads to the different behaviors between type A and type B. The auxiliary elements of type A lies orthogonal to the directional energy from the feed, while those of type B are aligned in the line 45° tilted to the feed slot. Therefore, more efficient antenna operations could be obtained for type A when locations of the auxiliary elements lies to the line orthogonal to feed's length.

For both antenna types, the FB ratio and deviation increases as the number of slots increases. With an increasing number of slots, the radiation pattern also becomes narrower with an increasing FB ratio. Figure 5c shows the Fourier-plane image obtained from one of the type-A antennas with the maximum FB ratio, and Figure 5d shows the corresponding simulation result. The radiation pattern is tilted slightly to the lower right-hand corner away from the axis passing through the centers of all the slots. The half power beamwidth (HPBW), which is defined by the angle between the half-power points of the main lobe in a plane, could not be directly measured due to the limited numerical aperture of the objective in the θ coordinate. A HPBW value of 71°, however, could be obtained from the simulated result. We note that the HPBW should be evaluated in the plane containing the maximum lobe intensity at $(\theta_{\text{max}}, \phi_{\text{max}}) = (56°, 347°)$, and we took the two −3-dB points from the same $\phi = 347°$ plane for the HPBW extraction.

In conclusion, we have demonstrated the first magnetic dipole feed-driven multislot nanoantenna for unidirectional free-space radiation in the visible wavelength range. We achieved a maximum FB ratio of 8.5 (9.2 dB) for a five-slot antenna. Even with the limited fabrication margins and a lack of methods for performing a full optimization, we were able to show that a

dx.doi.org/10.1021/nl500062f | Nano Lett. 2014, 14, 3072−3078

leading-order phase analysis can still be applied to the design of efficient aperture-type optical Yagi−Uda antennas. Better unidirectional radiation performance can be anticipated with further optimization of the antenna structures and materials.

Our optical antenna structure delivers a few structural advantages for integrated nanophotonic structures. First, SPPs can be directly injected to the antenna either by a thin metal layer or a metal−insulator−metal waveguide. Second, spatial separation owing to the metallic layer between the upper and the lower hemispheres allows a 3D optical via between physically separated layers. Third, the metal layer can be simultaneously used as electrodes for electrically excitable integrated optical devices. Other imminent subsequent works, based on this multislot nanoantenna structure, are a beam router driven by the polarization of the incident beam and slot antennas driven by local sources such as quantum dots or dye molecules. Elastic and inelastic single molecule spectroscopy using multislots is expected to provide new types of plasmonic enhancement that could lead to various chemistry and biology related research.

■ ASSOCIATED CONTENT

Supporting Information

Detailed explanation of the materials and methods, supporting figures, and details of the two-, three-, and five-slot antenna analysis. This material is available free of charge via the Internet at http://pubs.acs.org.

■ AUTHOR INFORMATION

Corresponding Authors

*E-mail: yeonsang.park@samsung.com (Y.P.).
*E-mail: chang-won.lee@samsung.com (C.-W.L.).

Author Contributions

§These authors contributed equally to this work.

Notes

The authors declare no competing financial interests.

■ ACKNOWLEDGMENTS

The authors are grateful to Prof. M. L. Brongersma at Stanford University for stimulating and fruitful discussions.

■ REFERENCES

(1) Biagioni, P.; Huang, J.-S.; Hecht, B. *Rep. Prog. Phys.* **2012**, *75*, 024402.
(2) Novotny, L.; van Hulst, N. *Nat. Photonics* **2011**, *5*, 83−90.
(3) Olmon, R. L.; Raschke, M. B. *Nanotechnology* **2012**, *23*, 444001.
(4) Garcia-Vidal, F. J.; Martin-Moreno, L.; Ebbesen, T. W.; Kuipers, L. *Rev. Mod. Phys.* **2010**, *82*, 729−787.
(5) Kinkhabwala, A.; Yu, Z.; Fan, S.; Avlasevich, Y.; Müllen, K.; Moerner, W. E. *Nat. Photonics* **2009**, *3*, 654−657.
(6) Knight, M. W.; Sobhani, H.; Nordlander, P.; Halas, N. J. *Science* **2011**, *332*, 702−704.
(7) Liu, N.; Mesch, M.; Weiss, T.; Hentschel, M.; Giessen, H. *Nano Lett.* **2010**, *10*, 2342−2348.
(8) Juan, M. L.; Righini, M.; Quidant, R. *Nat. Photonics* **2011**, *5*, 349−356.
(9) Jun, Y. C.; Huang, K. C. Y.; Brongersma, M. L. *Nat. Commun.* **2011**, *2*, 283:1−6.
(10) Kosako, T.; Kadoya, Y.; Hofmann, H. F. *Nat. Photonics* **2010**, *4*, 312−315.
(11) Curto, A. G.; Volpe, G.; Taminiau, T. H.; Kreuzer, M. P.; Quidant, R.; van Hulst, N. F. *Science* **2010**, *329*, 930−933.
(12) Dorfmüller, J.; Dregely, D.; Esslinger, M.; Khunsin, W.; Vogelgesang, R.; Kern, K.; Giessen, H. *Nano Lett.* **2011**, *11*, 2819−2824.
(13) Dregely, D.; Taubert, R.; Dorfmüller, J.; Vogelgesang, R.; Kern, K.; Giessen, H. *Nat. Commun.* **2011**, *2*, 267:1−7.
(14) Jackson, J. D. *Classical Electrodynamics*, 3rd ed.; Wiley: New York, 1998.
(15) Balanis, C. A. *Antenna Theory: Analysis and Design*, 3rd ed.; Wiley-Interscience: New York, 2005.
(16) Johnson, R. C.; Jasik, H. *Antenna Engineering Handbook*, 3rd ed.; McGraw-Hill: New York, 1993.
(17) Van Beijnum, F.; Rétif, C.; Smiet, C. B.; Liu, H.; Lalanne, P.; van Exter, M. P. *Nature* **2012**, *492*, 411−414.
(18) Taflove, A.; Hagness, S. C. *Computational Electrodynamics: The Finite-Difference Time-Domain Method*, 3rd ed.; Artech House: Boston, 2005.
(19) Demarest, K.; Huang, Z.; Plumb, R. *IEEE Trans. Antennas Propag.* **1996**, *44*, 1150−1157.
(20) Yi, J.-M.; Cuche, A.; de León-Pérez, F.; Degiron, A.; Laux, E.; Devaux, E.; Genet, C.; Alegret, J.; Martín-Moreno, L.; Ebbesen, T. W. *Phys. Rev. Lett.* **2012**, *109*, 023901.
(21) Rotenberg, N.; Spasenović, M.; Krijger, T. L.; le Feber, B.; García de Abajo, F. J.; Kuipers, L. *Phys. Rev. Lett.* **2012**, *108*, 127402.
(22) López-Tejeira, F.; Rodrigo, S. G.; Martín-Moreno, L.; García-Vidal, F. J.; Devaux, E.; Ebbesen, T. W.; Krenn, J. R.; Radko, I. P.; Bozhevolnyi, S. I.; González, M. U.; Weeber, J. C.; Dereux, A. *Nat. Phys.* **2007**, *3*, 324−328.
(23) Lezec, H. J.; Degiron, A.; Devaux, E.; Linke, R. A.; Martin-Moreno, L.; Garcia-Vidal, F. J.; Ebbesen, T. W. *Science* **2002**, *297*, 820−822.
(24) Collin, S.; Pardo, F.; Pelouard, J.-L. *Opt. Express* **2007**, *15*, 4310−4320.
(25) Novotny, L. *Phys. Rev. Lett.* **2007**, *98*, 266802.
(26) Degiron, A.; Lezec, H. J.; Yamamoto, N.; Ebbesen, T. W. *Opt. Commun.* **2004**, *239*, 61−66.
(27) García-Vidal, F. J.; Martín-Moreno, L.; Moreno, E.; Kumar, L. K. S.; Gordon, R. *Phys. Rev. B* **2006**, *74*, 153411.
(28) Kang, J. H.; Choe, J.-H.; Kim, D. S.; Park, Q.-H. *Opt. Express* **2009**, *17*, 15652−15658.
(29) López-Tejeira, F.; Rodrigo, S. G.; Martín-Moreno, L.; García-Vidal, F. J.; Devaux, E.; Dintinger, J.; Ebbesen, T. W.; Krenn, J. R.; Radko, I. P.; Bozhevolnyi, S. I.; González, M. U.; Weeber, J. C.; Dereux, A. *New J. Phys.* **2008**, *10*, 033035.
(30) Bahk, Y.-M.; Choi, J. W.; Kyoung, J.; Park, H. R.; Ahn, K. J.; Kim, D. S. *Opt. Express* **2012**, *20*, 25644−25653.
(31) Gordon, R.; Brolo, A. *Opt. Express* **2005**, *13*, 1933−1938.